



PAPER • OPEN ACCESS

## The effects of pressure on the lattice of the rare-earth-based perovskite-type oxides $\text{SmAlO}_3$ and $\text{NdAlO}_3$

To cite this article: Hui Li *et al* 2022 *New J. Phys.* **24** 113008

View the [article online](#) for updates and enhancements.

### You may also like

- [Frequency dependence of the quasi-soft Raman-active modes in rotationally distorted  \$\text{R}^{3+}\text{B}^{3+}\text{O}\_6\$  perovskites \( \$\text{R}^{3+}\$ —rare earth,  \$\text{B}^{3+}\$ —Al, Sc, Ti, V, Cr, Mn, Fe, Co, Ni, Ga\)](#)  
N D Todorov, M V Abrashev and V G Ivanov
- [Shubnikov–de Haas oscillations and nontrivial topological states in Weyl semimetal candidate  \$\text{SmAlSi}\$](#)   
Longmeng Xu, Haoyu Niu, Yuming Bai et al.
- [Effects of co-precipitation method on microwave dielectric properties of  \$0.7\text{CaTiO}\_3-0.3\text{SmAlO}\_3\$  ceramics](#)  
Huajian Hu, Chun-E Huang, Jing Nan et al.



## PAPER

The effects of pressure on the lattice of the rare-earth-based perovskite-type oxides  $\text{SmAlO}_3$  and  $\text{NdAlO}_3$ 

## OPEN ACCESS

RECEIVED  
26 April 2022REVISED  
8 October 2022ACCEPTED FOR PUBLICATION  
19 October 2022PUBLISHED  
3 November 2022

Original content from  
this work may be used  
under the terms of the  
[Creative Commons  
Attribution 4.0 licence](#).

Any further distribution  
of this work must  
maintain attribution to  
the author(s) and the  
title of the work, journal  
citation and DOI.

Hui Li<sup>1,2</sup>, Shuailing Ma<sup>2</sup>, Jili Ye<sup>1</sup>, Nana Li<sup>3,\*</sup> and Xin Wang<sup>2,\*</sup><sup>1</sup> College of Mathematics and Physics, Guangxi Minzu University, Nanning, 530006, People's Republic of China<sup>2</sup> State Key Laboratory of Superhard Materials, Jilin University, Changchun 130012, People's Republic of China<sup>3</sup> Center for High Pressure Science and Technology Advanced Research, Shanghai 201203, People's Republic of China

\* Authors to whom any correspondence should be addressed.

E-mail: [nana.li@hpstar.ac.cn](mailto:nana.li@hpstar.ac.cn) and [xin\\_wang@jlu.edu.cn](mailto:xin_wang@jlu.edu.cn)**Keywords:** perovskite, high pressure, structural phase transition, bulk modulusSupplementary material for this article is available [online](#)**Abstract**

This paper studies the behavior of  $\text{SmAlO}_3$  and  $\text{NdAlO}_3$  when they are subject to high pressures. This work is undertaken using angle-dispersive synchrotron x-ray powder diffraction and Raman spectroscopy at pressures up to 24.2 and 39.0 GPa, respectively. It is found that  $\text{SmAlO}_3$  undergoes an orthorhombic ( $Pnma$ ) to rhombohedral ( $R-3c$ ) structure transition at around 10 GPa; this transition is induced by the rotation of the  $\text{AlO}_6$  octahedra toward that of the ideal perovskite structure when the material is subject to high pressures. The tilting of the  $\text{AlO}_6$  octahedra also decreases at high pressures in  $\text{NdAlO}_3$ . It is found that  $\text{NdAlO}_3$  maintains its original rhombohedral structure for pressures of up to 39.0 GPa. The structural changes observed in these compounds help establish the electrical and magnetic properties of  $\text{RAIO}_3$  ( $R = \text{Sm}$  or  $\text{Nd}$ ) at high pressures.

**1. Introduction**

In recent decades, perovskites and their derivatives have become the focus of considerable research because of their useful properties, such as ferromagnetism, photocatalysis, optoelectronic, and superconductivity [1–6]. Intense research has been carried out on  $\text{ABO}_3$ -type perovskites subject to high pressure as better understanding of their physical properties is important for practical applications and is of fundamental interest to the condensed matter and physics communities.  $\text{TbMnO}_3$  has the largest known ferroelectric polarization among spin-driven ferroelectrics; this is induced by the magnetoelectric phase transition that occurs at high pressures [7]. The quenched nonmagnetic state of these  $\text{ABO}_3$ -type perovskites has been interpreted as a spin crossover, i.e. the transition of the  $\text{Fe}^{3+}$  ions from the high ( $S = 5/2$ ) to the low spin state ( $S = 1/2$ ) in  $\text{REFeO}_3$  ( $\text{RE} = \text{Pr}, \text{Eu}, \text{or Lu}$ ),  $\text{GaFeO}_3$ , and  $\text{BiFeO}_3$  [8–10]. To further understand the behavior that originates from the couplings between the electronic, magnetic, and structural properties of these materials, investigations into the structural changes that occur at high pressures are required. Two important structural modifications are observed in  $\text{ABO}_3$  perovskites: the tilting of the  $\text{BO}_6$  octahedra and cation displacements. Any changes in these two characteristics can cause a structural phase in  $\text{ABO}_3$  perovskites. For example,  $\text{BiFeO}_3$  shows two structural phase transitions; one occurs at 3 GPa and the second at pressures greater than 10 GPa. The first structural change occurs when the rhombohedrally distorted perovskite transitions to a distorted monoclinic structure, as characterized by the superimposition of tilts and cation displacements. Subsequently, the distorted monoclinic structure transforms into a nonpolar orthorhombic  $Pnma$  structure due to cation displacements in  $\text{BiFeO}_3$  [8, 11, 12].  $\text{LaAlO}_3$  and  $\text{PrAlO}_3$  have been observed to exhibit a decrease of the lattice distortion and a decrease in the tilts of the  $\text{AlO}_6$  octahedra, which lead to a rhombohedral-to-cubic phase transition, when subject to high pressures [13, 14].

For rare-earth-based perovskite-type oxides  $\text{REAlO}_3$  ( $\text{RE} = \text{rare earth}$ ), aluminates with perovskite structure are formed from La to Lu, with varying physical and chemical properties [15]. Due to the different

radii of rare earth atoms, the different rare earth elements form perovskite structure with different levels of distortion within the lattice. Typically,  $\text{SmAlO}_3$  exhibits an orthorhombic symmetry and  $\text{NdAlO}_3$  shows a rhombohedral symmetry at ambient pressure and room temperature.  $\text{SmAlO}_3$  and  $\text{NdAlO}_3$  have been the subject of considerable research due to their excellent physical properties; these materials are widely used as a substrate for superconducting devices [16–18]. As an important oxygen ion conductor, they also represent a promising electrolyte for use in solid-oxide fuel cells [19]. Pressure and temperature are key parameters in determining their physical properties. For instance, studies on the temperature dependences of the structural phase transition of these materials have revealed different process in these compounds. When subject to increases in temperatures,  $\text{SmAlO}_3$  shows two structural phase transitions; first the materials transitions from having a orthorhombic structure to a rhombohedral geometry, and subsequently it shows a transitions to a cubic phase [20–22]. As for  $\text{NdAlO}_3$ , the phase transition from a rhombohedral structure to a cubic geometry occurs at a temperature of approximately 2180 K [23]. A high pressure can also modify the mechanical and electronic properties of the materials; these changes are induced by the pressure changing the interatomic distances within the structure. Here we present an in-situ investigation into the structural changes that occur in  $\text{REAlO}_3$  ( $\text{RE} = \text{Sm}$  or  $\text{Nd}$ ) when it is subject to high pressures.

## 2. Experimental details

The raw materials used in this study are  $\text{Sm}_2\text{O}_3$  (99.99% purity),  $\text{Nd}_2\text{O}_3$  (99.99% purity),  $\text{Al}(\text{NO}_3)_3 \cdot 9\text{H}_2\text{O}$  (99.99% purity), and citric acid (AR). The  $\text{SmAlO}_3$  was synthesized using the subsequent procedure: first  $\text{Sm}_2\text{O}_3$  was dissolved into nitric acid and distilled water was added to yield a dilute Sm nitrate solution.  $\text{Al}(\text{NO}_3)_3 \cdot 9\text{H}_2\text{O}$  was then added to the distilled water and mixed with the Sm nitrates following a stoichiometric ratio of  $\text{Sm}:\text{Al} = 1:1$ . The citric acid was then added to obtain a solution with a citrate acid/nitrate ratio of 1.2. A magnetic agitator was then used to ensure continuous stirring of the mixed solution. The temperature of the solution was increased to 353 K to induce evaporation until a sticky brown gel was generated. The gel was then baked at 423 K and subsequently calcined at a temperature of 1473 K for 10 h in an air atmosphere by intermediate grinding and pelletizing. The preparation of  $\text{NdAlO}_3$  followed a similar procedure to that used in the preparation of  $\text{SmAlO}_3$ .

Powder x-ray diffraction (XRD) was performed to measure the phase purity (Rigaku Rotaflex x-ray diffractometer) using a  $\text{Cu-K}\alpha$  radiation source under normal conditions. The high-pressure XRD measurement was conducted using an angle-dispersive synchrotron radiation source at the beamline X17C of the National Synchrotron Light Source, Brookhaven National Laboratory, USA. A symmetric diamond anvil cell (DAC) with an anvil culet of 300  $\mu\text{m}$  was utilized to generate the high-pressure conditions using T301 stainless steel as the gasket, which was preindented to a thickness of 40  $\mu\text{m}$ . The as-prepared sample together with a small piece of ruby which acted as the pressure calibrant [24], and a 4:1 methanol/ethanol mixture for use as a pressure-transmitting medium were then loaded into the DACs. The experimental parameters including the distance between sample and detector were calibrated using  $\text{CeO}_2$  (a standard material). The software FIT2D was used to convert the information regarding the image plates into intensity versus diffraction angle  $2\theta$  patterns. The high-pressure Raman spectra were obtained using a Raman spectrometer and a 532 nm excitation laser at a power of 3 mW. The preparation of the DACs and loading samples followed the same techniques as those used for the high-pressure XRD experiments. To exclude the effects of deviatoric stress caused by nonhydrostatic effects, Ne was used as the pressure-transmitting medium in the high-pressure Raman measurements.

## 3. Results and discussion

### 3.1. XRD results at ambient pressure

We found that  $\text{SmAlO}_3$  has an orthorhombic structure with a  $Pnma$  space group at room temperature, which is in agreement with the previous reports [25, 26]. As shown in the inset of figure 1(a), it can be regarded as a three-dimensional  $\text{AlO}_6$  network with the interstitial spaces occupied by Sm atoms. Like  $\text{LaAlO}_3$ ,  $\text{NdAlO}_3$  has a rhombohedral structure with  $R\bar{3}c$  space group at room temperature; this structure is shown in the inset of figure 1(b) [23, 27, 28]. The distorted rhombohedral structure shows an antiphase  $a^- a^- a^-$  (tilt system in Glazer's notation) tilt of the adjacent octahedra, whereas the distortions of the orthorhombic structure have the combined  $a^- a^- c^+ / a^- a^- c^-$  octahedral tilting [29].

The refinement of ambient-pressure diffraction patterns was realized using the Rietveld method and the generalized structure analysis system (GSAS) software [30].  $\text{SmAlO}_3$  and  $\text{NdAlO}_3$  were refined in the  $Pnma$  phase with the lattice constants of  $a = 5.2991(8)$  Å,  $b = 7.4767(8)$  Å, and  $c = 5.2966(9)$  Å, and the  $R\bar{3}c$  phase with  $a = b = 5.3183(2)$  Å and  $c = 12.9244(7)$  Å. Figure 1 presents the refined patterns of

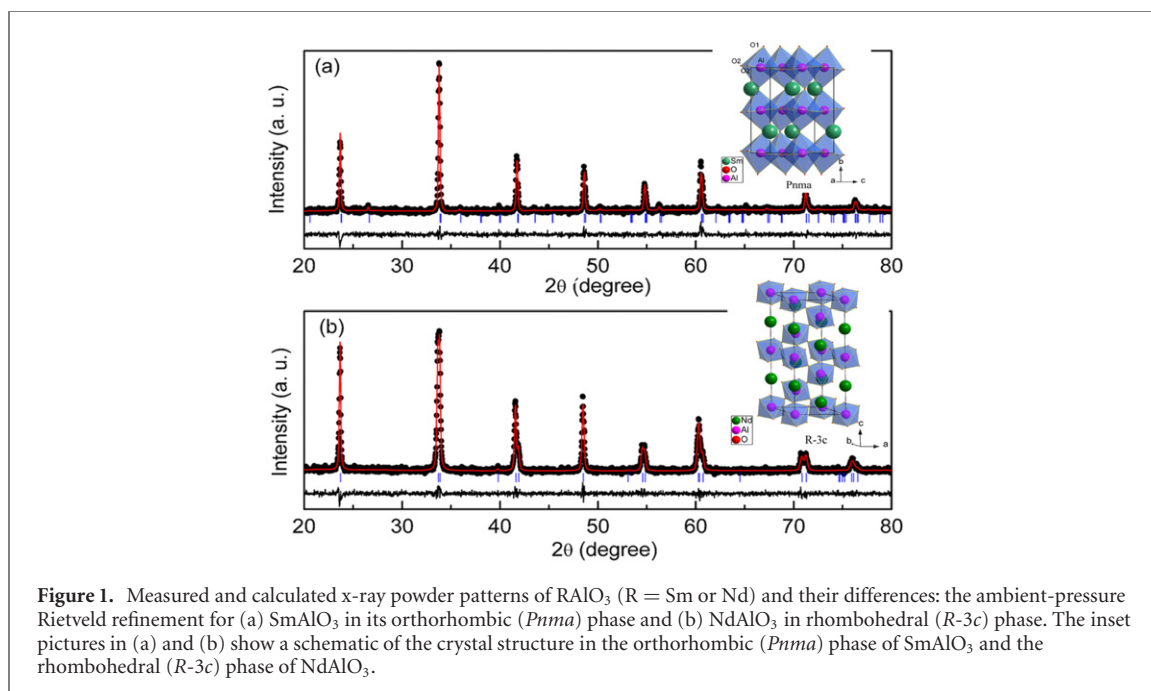


**Figure 1.** Measured and calculated x-ray powder patterns of  $\text{REAlO}_3$  ( $\text{R} = \text{Sm}$  or  $\text{Nd}$ ) and their differences: the ambient-pressure Rietveld refinement for (a)  $\text{SmAlO}_3$  in its orthorhombic ( $Pnma$ ) phase and (b)  $\text{NdAlO}_3$  in rhombohedral ( $R-3c$ ) phase. The inset pictures in (a) and (b) show a schematic of the crystal structure in the orthorhombic ( $Pnma$ ) phase of  $\text{SmAlO}_3$  and the rhombohedral ( $R-3c$ ) phase of  $\text{NdAlO}_3$ .

**Table 1.** Structural information related to  $\text{SmAlO}_3$  and  $\text{NdAlO}_3$  at room temperature and ambient pressure.

Compounds	$\text{SmAlO}_3$	$\text{NdAlO}_3$
Crystal type	Orthorhombic	Rhombohedral
Space group	$Pnma(62)$	$R-3c(167)$
$a/\text{\AA}$	5.2991(8)	5.3183(2)
$b/\text{\AA}$	7.4767(8)	5.3183(2)
$c/\text{\AA}$	5.2966(9)	12.9244(7)
Atoms position	Wyckoff ( $xyz$ )	Wyckoff ( $xyz$ )
Al	$4b(0.5\ 0\ 0)$	$6b(0\ 0\ 0)$
Sm/Nd	$4c(0.0244(9)\ 0.25\ 0.9913(4))$	$6a(0\ 0\ 0.25)$
O(1)	$4c(0.4858(5)\ 0.25\ 0.0411(7))$	$18e(0.5355(6)\ 0\ 0.25)$
O(2)	$8d(0.3022(5)\ 0.0462(5)\ 0.6720(6))$	
Residuals <sup>a</sup> /%	$R_{\text{wp}}: 6.05\%$ $R_{\text{p}}: 4.78\%$	$R_{\text{wp}}: 6.46\%$ $R_{\text{p}}: 5.13\%$

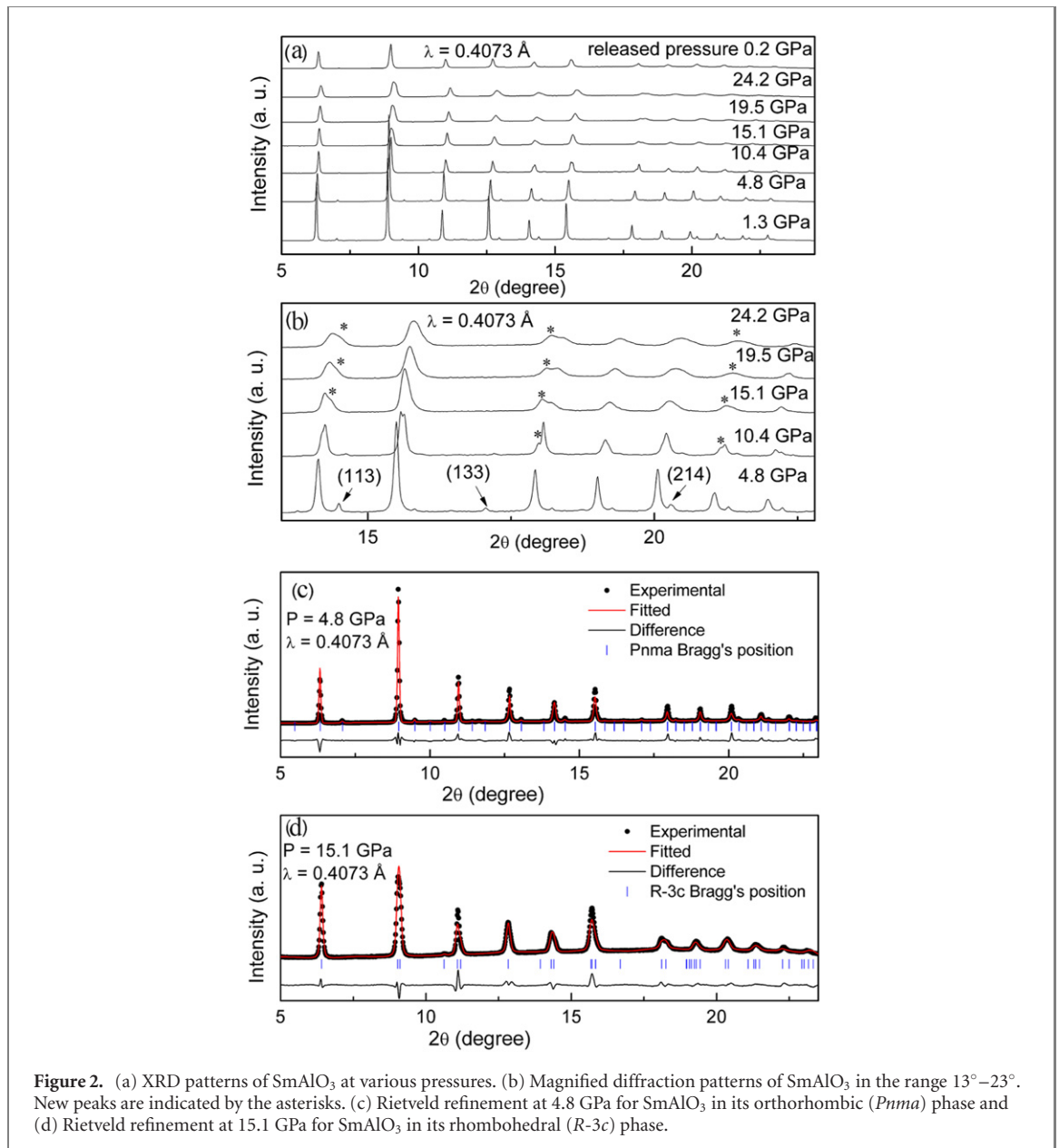
<sup>a</sup> $R_{\text{wp}}$  and  $R_{\text{p}}$  as defined in the GSAS software [30].

$\text{REAlO}_3$  ( $\text{RE} = \text{Sm}$  or  $\text{Nd}$ ) and the computed patterns, together with their differences and the refinement merits. Table 1 lists the refined atomic position coordinates.

### 3.2. The lattice evolution of $\text{SmAlO}_3$ at high pressures

A high-pressure synchrotron powder XRD experiment was performed to reveal the structural behaviors of  $\text{SmAlO}_3$ . The XRD patterns were recorded at with the samples subject to a set of pressures up to 24.2 GPa. Figures 2(a) and (b) present some of the measured and enlarged typical powder diffraction patterns of  $\text{SmAlO}_3$ , respectively. The original phase can be seen to exhibit new peaks at 10.4 GPa; at this pressure the ethanol–methanol pressure-transmitting medium is known to become solid giving rise to nonhydrostatic conditions [31]. However, it is known that the these stresses can induce peak broadening effects; significant changes are observed in the multiplicity and the relative intensity of the Bragg reflection peaks, as shown in the enlarged patterns depicted in figure 2(b). The intensity of reflection peaks of (113), (133), and (214) of the original phase start to decrease at a pressure of 10.4 GPa and disappear at around 15.1 GPa. These findings indicate that a structural phase transition is initiated at a pressure above 10.4 GPa and is completed at around 15.1 GPa. Upon releasing the pressure, the original phase was obtained. The orthorhombic  $\text{SmAlO}_3$  was refined for all pressures below 10.4 GPa by the previous method. The results shown in figure 2(c) present the Rietveld refinement result at 4.8 GPa with  $R_{\text{p}} = 6.52\%$  and  $R_{\text{wp}} = 4.48\%$ .

In the case of  $\text{ABO}_3$  with  $M_{\text{A}}/M_{\text{B}} > 1$ , Zhao *et al* [32, 33] found that the temperature of zone-boundary phase transition,  $T_{\text{C}}$ , decreases with increasing pressure, (i.e.  $dT_{\text{C}}/dP < 0$ ). In this work, the site parameter,



$M_i$ , was defined as:

$$M_i = (R_i N_i / B) \exp\left(\frac{R_0 - R_i}{B}\right), \quad (1)$$

where  $N_i$ ,  $R_i$ ,  $R_0$ , and  $B$  represent the coordination number, the average bond length at ambient pressure, the bond-valence parameters, and the universal constant (0.37 Å), respectively [33]. It was found that LaAlO<sub>3</sub> with  $M_A/M_B > 1$  underwent a rhombohedral-to-cubic phase transition at a pressure of approximately 14 GPa [13]. The same transition was also observed in NdNiO<sub>3</sub> at 6 GPa [34]. Similarly, LaGaO<sub>3</sub> underwent an orthorhombic-to-rhombohedral phase transition around 2.5 GPa [35]. In these perovskites, the same phase transitions could be observed as a result of increasing temperature [23, 36–38]. In the case of SmAlO<sub>3</sub> with  $M_A/M_B > 1$ , the first phase transition from an orthorhombic to a rhombohedral structure occurred within the temperature range of 1023–1058 K [21, 22]. As discussed from above, SmAlO<sub>3</sub> is also expected to undergo a phase transition from an orthorhombic (*Pnma*) to a rhombohedral (*R-3c*) structure when the material is subject to high pressure. The structural phase transition observed in SmAlO<sub>3</sub> occurs at 10.4 GPa. The Rietveld refinement results indicate that SmAlO<sub>3</sub> is completely transformed into a rhombohedral phase at a pressure of 15.1 GPa, as shown in figure 2(d) with  $R_p = 5.01\%$  and  $R_{wp} = 3.17\%$ . The result obtained in the case of SmAlO<sub>3</sub> show in good agreement with the predictions. Angel *et al* [39] and Ross *et al* [40] developed a novel bond-valence matching relation-based method for predicting the changes in GdFeO<sub>3</sub>-type orthorhombic perovskites structures at high pressures. It was shown that the BO<sub>6</sub> octahedra became less tilted and the symmetry of the structure increased when

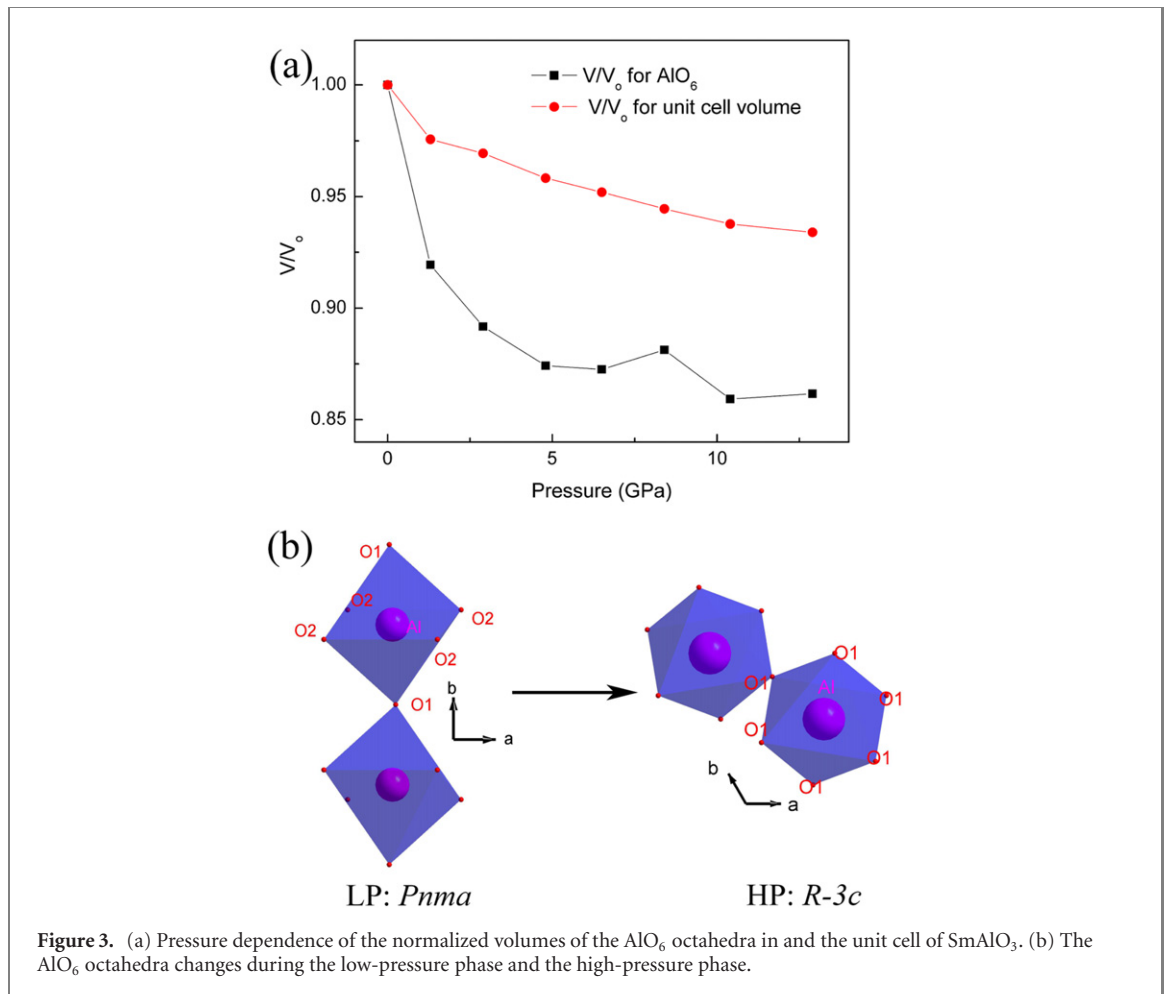


**Figure 3.** (a) Pressure dependence of the normalized volumes of the  $\text{AlO}_6$  octahedra in and the unit cell of  $\text{SmAlO}_3$ . (b) The  $\text{AlO}_6$  octahedra changes during the low-pressure phase and the high-pressure phase.

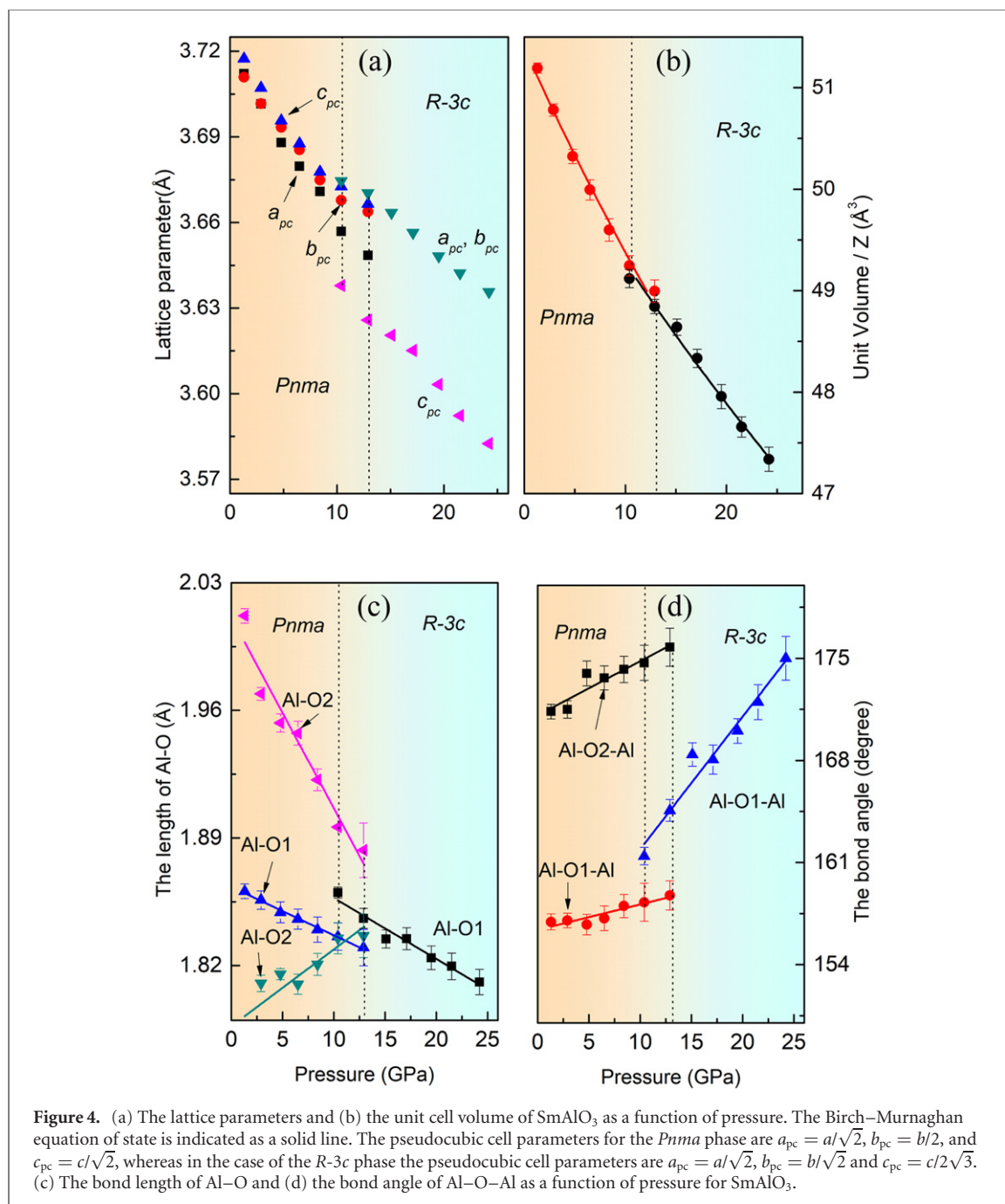
the  $\text{BO}_6$  octahedra were more susceptible to compression than the  $\text{AO}_{12}$  polyhedra under high pressures. The structure was predicted to evolve toward lower symmetry configurations when the  $\text{AO}_{12}$  polyhedra were more susceptible to compression than the  $\text{BO}_6$  octahedra under a pressure loading [33, 41]. This prediction was in good agreement with other studied orthorhombic perovskites, such as  $\text{TbMnO}_3$ ,  $\text{GdMnO}_3$ ,  $\text{LaMnO}_3$ ,  $\text{GdAlO}_3$ , and  $\text{YAlO}_3$  [40, 42–45]. The normalized volume change of the  $\text{AlO}_6$  octahedra in  $\text{SmAlO}_3$  is more susceptible to compression than the unit cell for pressures below 15.1 GPa, as shown in figure 3(a). This suggests that the symmetry of the structure of  $\text{SmAlO}_3$  increases at high pressures. It also provides the evidence for the transition from the low symmetry ( $Pnma$ ) phase to the high symmetry ( $R-3c$ ) phase. Since the octahedral distortions in the  $\text{ABO}_3$ -type oxides are crucial in the process of structural phase transitions, we can conclude that the observed structural phase transition in  $\text{SmAlO}_3$  is induced by the  $\text{AlO}_6$  octahedra rotation toward the that of the ideal perovskite structure under high pressures. Figure 3(b) shows the changes in the  $\text{AlO}_6$  octahedra in the low-pressure and high-pressure phases.

The pressure dependence of the lattice parameters (a pseudocubic cell is adopted) of  $\text{SmAlO}_3$  at pressures up to 24.2 GPa are shown in figure 4. The cell parameter,  $c_{\text{pc}}$ , exhibits anomalous behavior above 12.9 GPa due to the nonhydrostatic conditions that are induced [46]. The volume of the unit cell of  $\text{SmAlO}_3$  decreases smoothly with increasing pressure. The state equation was fitted with the following 3rd-order Birch–Murnaghan state equation,

$$P = \frac{3.0}{2}B_0 \left[ \left( \frac{V_0}{V} \right)^{\frac{7}{3}} - \left( \frac{V_0}{V} \right)^{\frac{5}{3}} \right] \times \left\{ 1 + \frac{3.0}{4}(B'_0 - 4) \times \left[ \left( \frac{V_0}{V} \right)^{\frac{2}{3}} - 1 \right] \right\}, \quad (2)$$

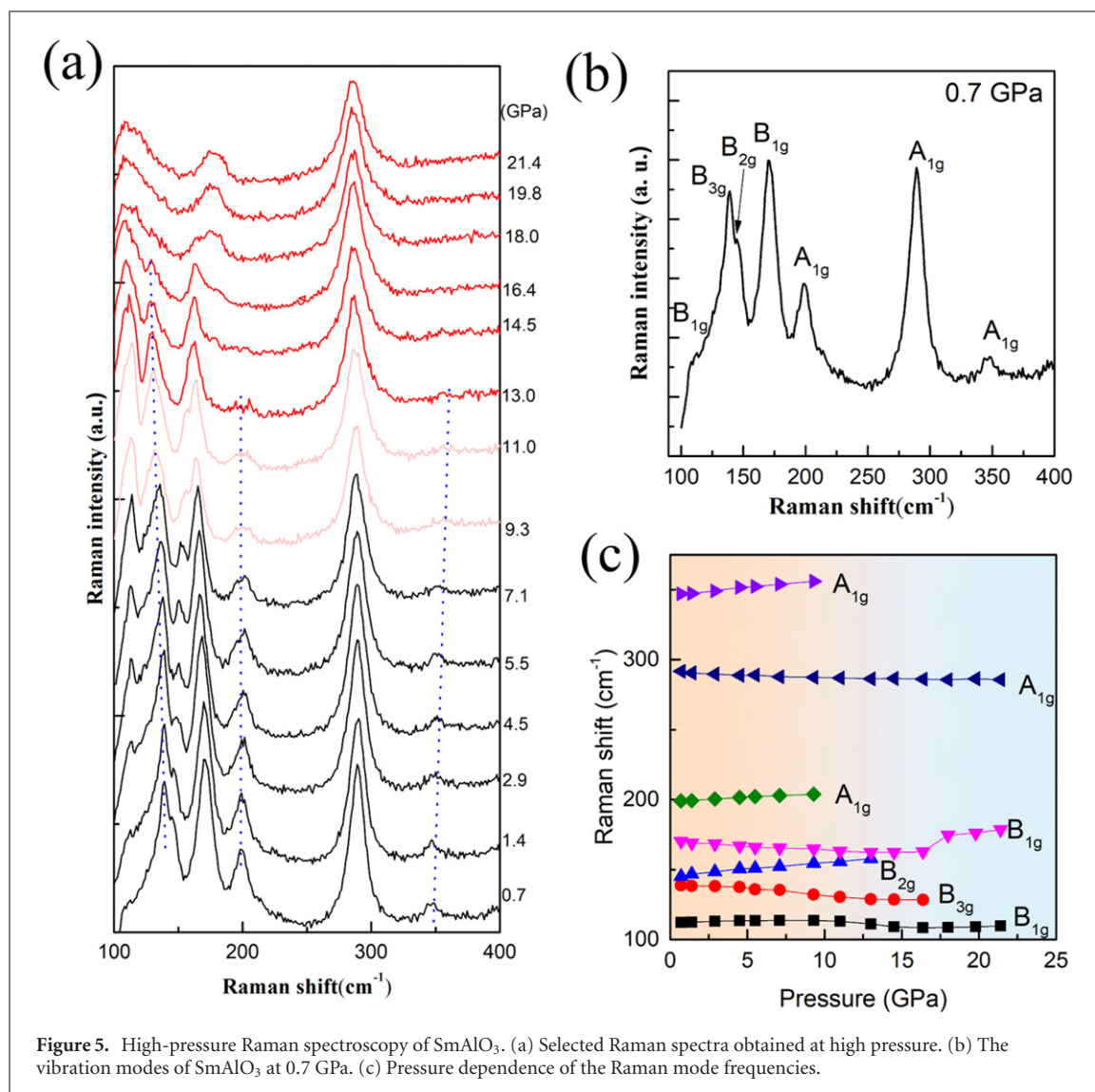
where  $B_0$  is the bulk modulus and  $B'_0$  is its pressure derivative at the equilibrium volume,  $V_0$ . By fitting the equation, we obtained  $B_0 = 223(10)$  GPa and  $B'_0 = 4$  (fixed) for  $V_0 = 51.42(11)$   $\text{\AA}^3$  for the orthorhombic ( $Pnma$ ) phase and  $B_0 = 262(9)$  GPa and  $B'_0 = 4$  (fixed) for  $V_0 = 51.18(10)$   $\text{\AA}^3$  for the rhombohedral ( $R-3c$ ) phase.

The high-pressure structural evolution was further investigated by evaluating the Al–O bond length and the Al–O–Al bond angle as a function of pressure (figure 4). The  $\text{AlO}_6$  octahedra generate three Al–O bond



pairs. Figure 1(a) shows that one pair (Al–O1) is aligned with the  $b$ -axis, and the remaining short Al–O2 bond and the long Al–O2 bond are located in the  $ac$ -plane. The rotations of the  $\text{AlO}_6$  octahedra generate two distinct Al–O–Al angles. One Al–O2–Al tilting angle is in the  $ac$ -plane and the other Al–O1–Al tilting angle is aligned with the  $b$ -axis. As shown in figure 4(c), the lengths of the Al–O1 bond and the longer Al–O2 bond shortens as the shorter Al–O2 bond length increases as a result of increasing pressure. The three Al–O bond pairs are equal in length at 15.1 GPa. The Al–O–Al bond angles increases with increasing pressure [figure 4(d)]. This implies that the tilting of the two neighboring  $\text{AlO}_6$  octahedra both along the  $b$ -axis and in the  $ac$ -plane decrease at high pressures. These results combined indicate that the  $\text{AlO}_6$  octahedra become less tilted when the material is subject to high pressures. It also indicates that the lattice distortion decreases at high pressures.

To exclude the effects of deviatoric stress caused by nonhydrostatic pressures, we also undertook high-pressure Raman spectroscopy using Ne as the pressure-transmitting medium; the results are shown in figure 5. In the  $Pnma$  structure, there are 24 Raman active modes:  $7A_{1g} + 7B_{1g} + 5B_{2g} + 5B_{3g}$ . In the range  $100\text{--}400\text{ cm}^{-1}$ , we observed seven Raman modes, as shown in figure 5(a). We obtained the vibration modes, as shown in figure 5(b).



The Raman peak of the A<sub>1g</sub> mode around 200 and 345 cm<sup>-1</sup> corresponds to a rotation about the  $y$ -axis of the Sm atoms and a stretching mode in the direction parallel to the  $x$ -axis of the O1 atom in SmAlO<sub>3</sub>. The B<sub>3g</sub> mode that is observed at around 139 cm<sup>-1</sup> corresponds to a rotation about the  $z$ -axis of the Sm atoms. The B<sub>1g</sub> mode situated at around 110 and 170 cm<sup>-1</sup>, and the A<sub>1g</sub> mode at around 287 cm<sup>-1</sup> correspond to a rotation of the AlO<sub>6</sub> octahedra. The B<sub>2g</sub> mode around 144 cm<sup>-1</sup> corresponds to a rotation of Sm atoms about the  $x$ -axis [47–50].

With increasing pressure, the intensity of the B<sub>1g</sub> mode situated at around 110 cm<sup>-1</sup> and the A<sub>1g</sub> mode at around 200 and 345 cm<sup>-1</sup> decreased at a pressure of 9.3 GPa and disappeared completely around 18.0 GPa, as shown in figure 5(a). This indicates that a structural phase transition occurs at approximately 9.3 GPa, which is consistent with the XRD results obtained for SmAlO<sub>3</sub>. However, the Raman spectroscopy results suggest that the structural phase transition of SmAlO<sub>3</sub> is completed at a pressure of around 18.0 GPa; this pressure is higher than that obtained from the high-pressure XRD results (15.1 GPa). A primary reason for this discrepancy is the different pressure-transmitting medium used in these studies. This difference is due to the fact that hydrostatic loading induced by the methanol–ethanol mixture can be maintained up to 10 GPa, whereas the Ne can maintain hydrostatic loading up to 20 GPa [51, 52]. We also note that Raman spectroscopy is more sensitive than powder XRD when it comes to distinguishing the small difference between the *Pnma* and *R-3c* space groups in the RAlO<sub>3</sub> systems.

Figure 5(c) summarizes the Raman shift changes that occur as a result of changes in pressure. The A<sub>1g</sub> mode at around 287 cm<sup>-1</sup> and B<sub>1g</sub> mode around 170 cm<sup>-1</sup> soften continuously with increasing pressure up to a pressure of 9.3 GPa; this indicates a decrease in the octahedral tilt angle with increasing pressure. This finding is consistent with the XRD results, as shown in figure 4(d). Compared with the Raman curves of LaAlO<sub>3</sub> and NdAlO<sub>3</sub> with its rhombohedral structure at ambient pressure and room temperature [13],

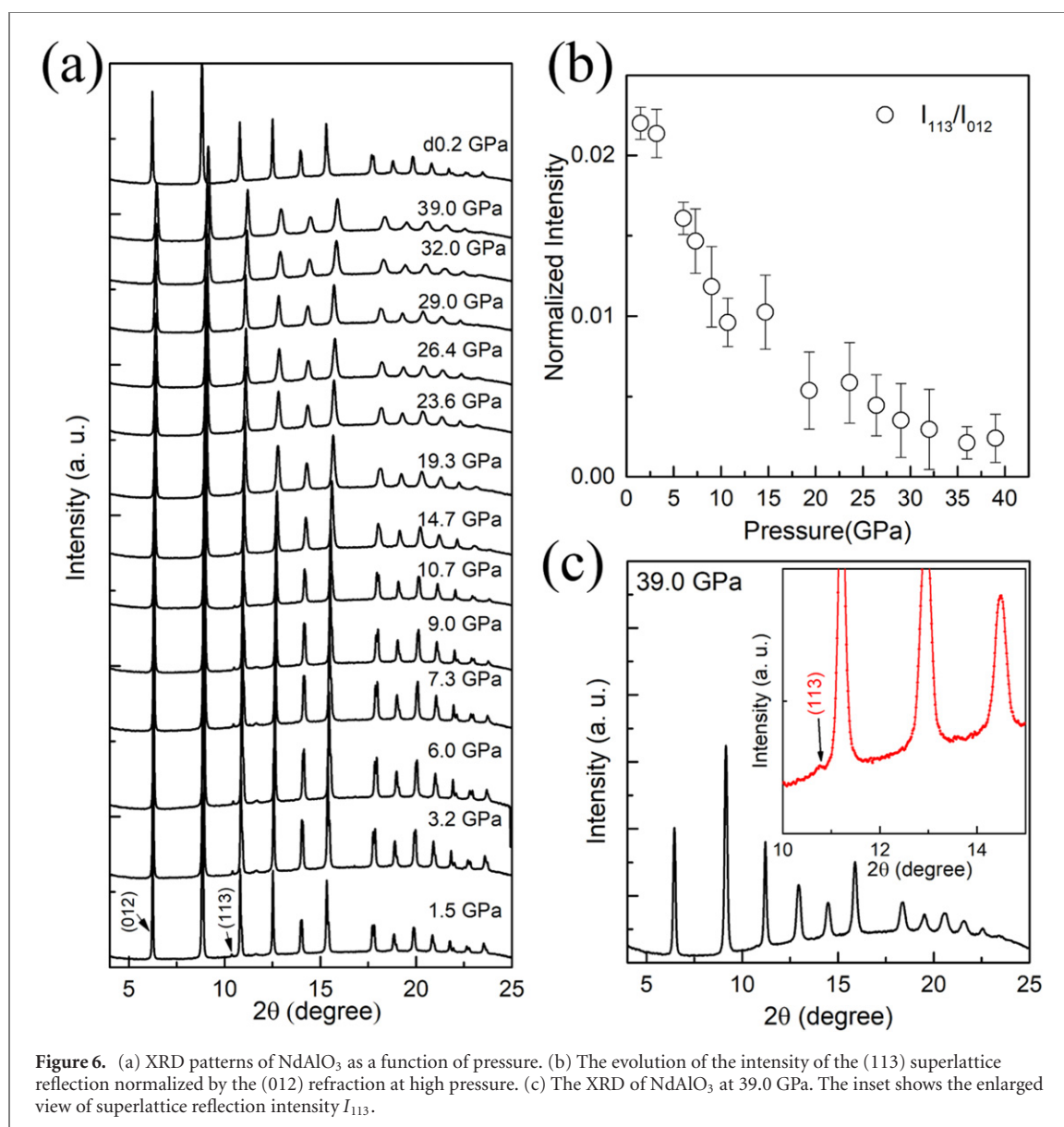


**Figure 6.** (a) XRD patterns of NdAlO<sub>3</sub> as a function of pressure. (b) The evolution of the intensity of the (113) superlattice reflection normalized by the (012) reflection at high pressure. (c) The XRD of NdAlO<sub>3</sub> at 39.0 GPa. The inset shows the enlarged view of superlattice reflection intensity  $I_{113}$ .

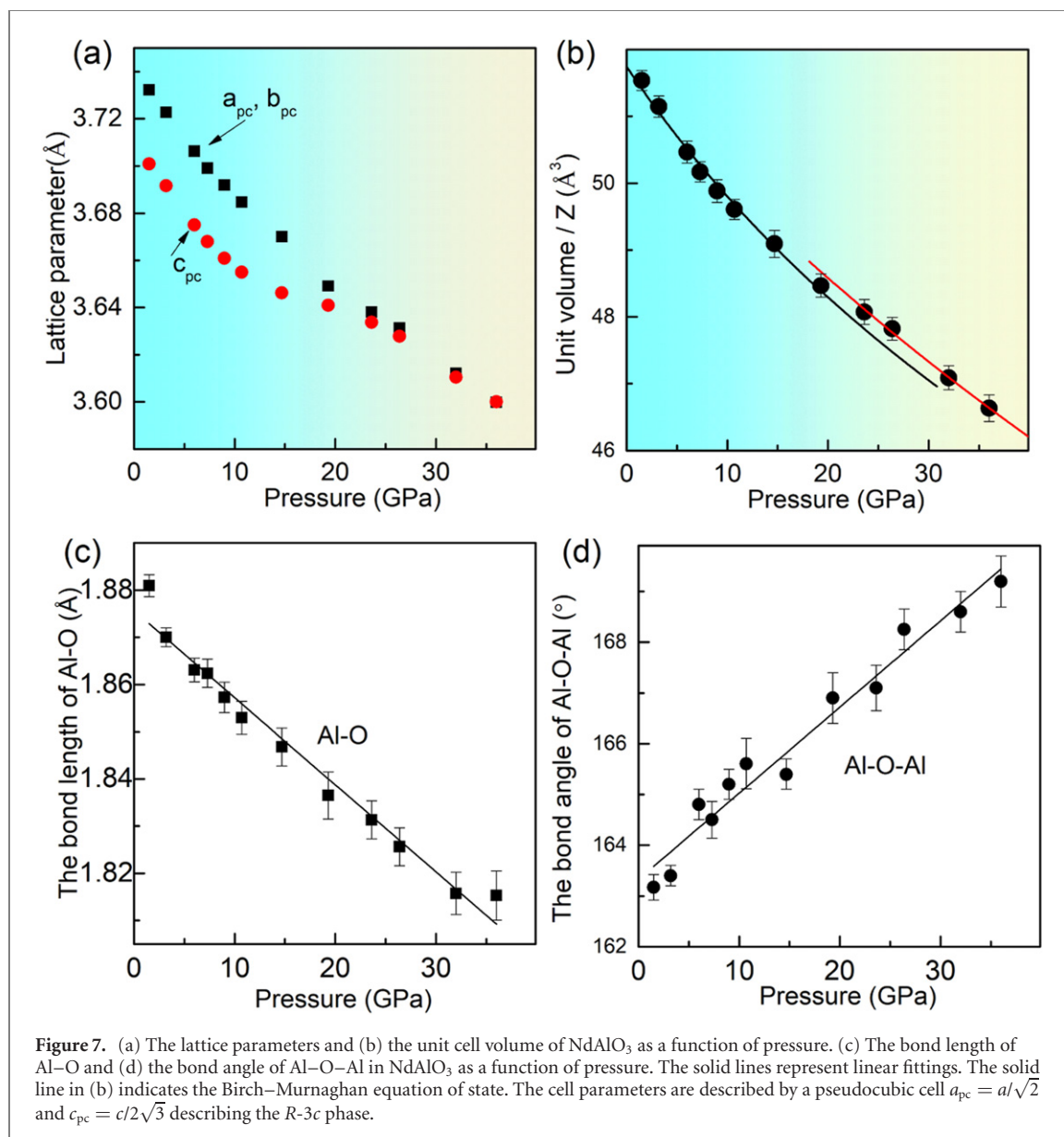
SmAlO<sub>3</sub> shows a structural phase transition from orthorhombic-to-rhombohedral symmetry at a pressure of around 9.3 GPa, which is consistent with the XRD results obtained here.

### 3.3. The lattice evolution of NdAlO<sub>3</sub> at high pressures

Theoretical calculation suggested the existence of a rhombohedral-to-cubic phase transition at a pressure of above 80 GPa [53]. In our study, we obtained the XRD patterns of NdAlO<sub>3</sub> for pressures up to 39.0 GPa, as shown in figure 6(a).

To investigate the possible structural phase transition, we induced the intensity change of one superlattice reflection,  $I_{113}$ , which is associated with the  $a^-a^-a^-$ -type rotation of the oxygen octahedra [13], as shown in figure 6(b). The normalized intensity of  $I_{113}/I_{012}$  decreased with increasing pressure, indicating the possibility of a phase transition from a rhombohedral-to-cubic structure. Unlike LaAlO<sub>3</sub> [13], the Bragg peak (113) is maintained up to pressures of 39.0 GPa, as shown in figure 6(c), which suggests that the rhombohedral structure remains in the case of NdAlO<sub>3</sub> up to the maximum pressure considered in our study.

To obtain the lattice parameters and the state equation, the refinements of the rhombohedral phase of NdAlO<sub>3</sub> were investigated using the GSAS software under the pressures considered in this work. The fitted pattern at a pressure of 19.3 GPa with  $R_p = 2.48\%$  and  $R_{wp} = 1.43\%$  is shown in figure S1. Figures 7(a) and (b) present the lattice parameters of NdAlO<sub>3</sub> as a function of pressure considering a pseudocubic cell. Interestingly, the P–V curve shows a discontinuity; this discontinuity is obtained by fitting two sets of P–V data separately for pressures below and above 19 GPa. This finding may be affected by the changes in lattice vibration which is related to the high-pressure Raman study presented below. We observed  $B_0 = 230(10)$



GPa and  $B'_0 = 6.7$  for  $V_0 = 310.456(5) \text{ \AA}^3$  for a pressure of 19 GPa. For pressures above 19 GPa, we measured  $B_0 = 301(16)$  GPa and  $B'_0 = 3.4$  for  $V_0 = 309.523(10) \text{ \AA}^3$ . The obtained bulk modulus is slightly higher than those observed in other perovskite oxides, such as YAlO<sub>3</sub>, PrAlO<sub>3</sub>, and LaAlO<sub>3</sub> whose bulk moduli are equal to 192(2), 193.0 (1.2), and 190 (5) GPa, respectively [13, 14, 46].

As shown in figure 7(a), the lattice parameters of NdAlO<sub>3</sub> decrease smoothly with increasing pressure. Interestingly, the values of  $a$  and  $c$  gradually converge for pressures above 20 GPa. This is likely to be caused by two factors: the peak broadening in the XRD patterns at high pressure and the existence of a higher structural symmetry that is reached by the decreasing of the AlO<sub>6</sub> octahedra tilting at high pressure. To further investigate the crystal structure of NdAlO<sub>3</sub>, we investigated the Al–O bond length and Al–O–Al bond angle of NdAlO<sub>3</sub> as a function of pressure; the findings are shown in figures 7(c) and (d). The Al–O bond length decreases as the Al–O–Al bond angles increase with increasing pressure. This suggests that the tilting of the AlO<sub>6</sub> octahedra decreases at high pressures, as is the case in SmAlO<sub>3</sub>.

To obtain insight into the crystal structural changes in NdAlO<sub>3</sub> at high pressure, we also undertook high-pressure Raman spectroscopy using Ne as the pressure-transmitting medium; the results are shown in figure 8. In the  $R-3c$  structure, there are 5 Raman active modes:  $A_{1g} + 4E_g$ . Major peaks can be assigned as follows: the band at  $240 \text{ cm}^{-1}$  of the  $A_{1g}$  mode is related to the rotation of the O octahedra; the two bands at  $163$  and  $513 \text{ cm}^{-1}$  of the  $E_g$  mode are associated with the vibration of the Nd atoms and the bending vibration of O atoms, respectively; the band at  $590 \text{ cm}^{-1}$  of the  $E_g$  mode is related to the out of phase stretching vibration of O atoms [54–56]. The forbidden Raman modes observed at around  $380$  and  $700 \text{ cm}^{-1}$  may be related to the vibrations of the Nd<sup>3+</sup> ions [56].

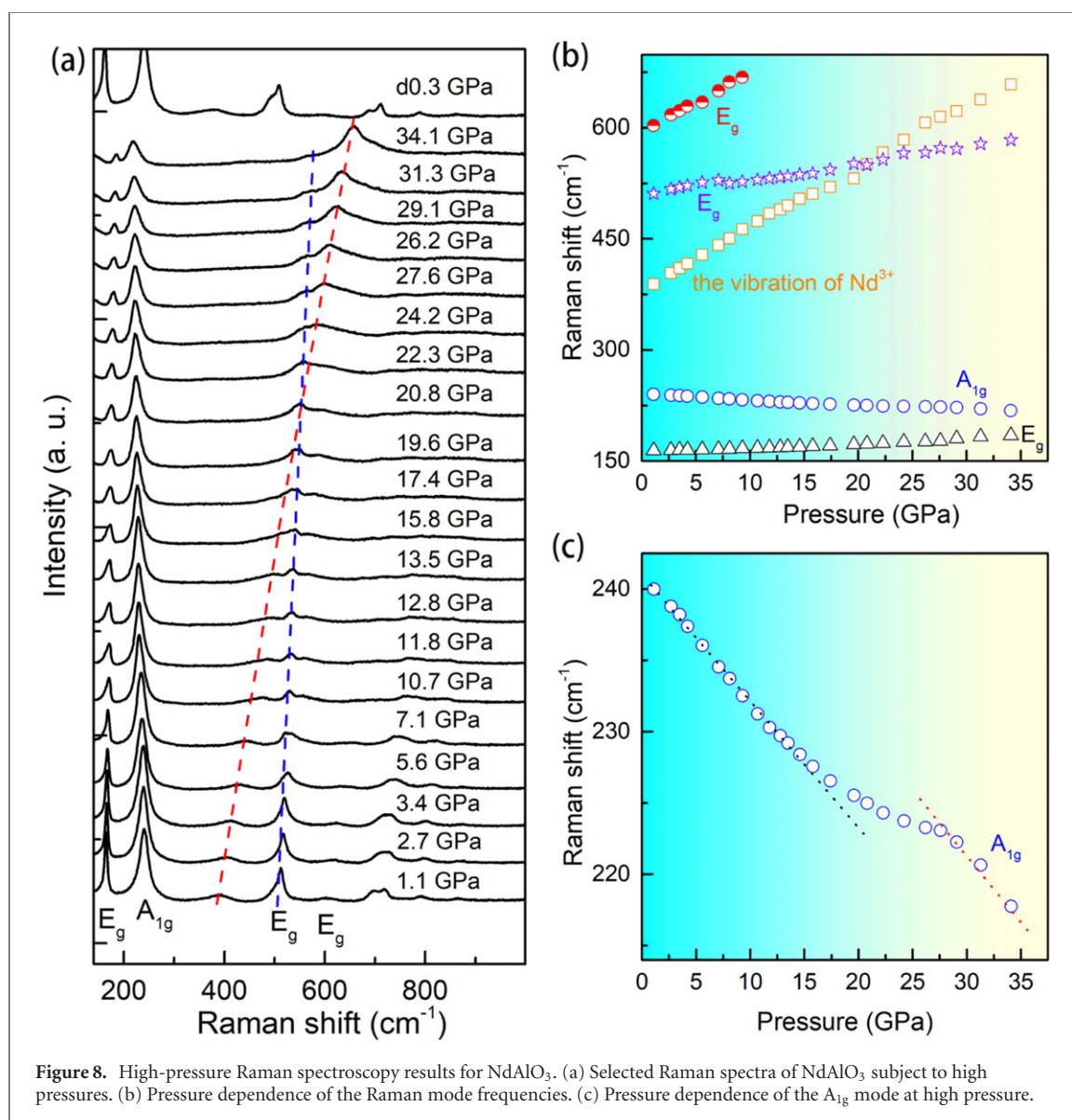


Figure 8(b) summarizes the Raman shifts that occur with changes in pressure. The Raman peak at 240 cm<sup>-1</sup> of the A<sub>1g</sub> mode softens continuously with increasing pressure, which is similar to the behavior observed in the A<sub>1g</sub> mode of LaAlO<sub>3</sub> and PrAlO<sub>3</sub> subject to high pressure [13, 14]. This is induced by a decrease in the octahedral tilt angle with increasing pressure; these findings are consistent with the XRD results as shown in figure 7(d). Unlike LaAlO<sub>3</sub> and PrAlO<sub>3</sub>, the A<sub>1g</sub> mode does not disappear or harden with further increasing pressure for pressures up to 34.1 GPa; this illustrates the existence of the original rhombohedral structure. The frequency of the A<sub>1g</sub> mode also shows discontinuity between 17.4 and 27 GPa, as shown in figure 8(c). The hydrostatic pressure conditions imposed by Ne can be maintained up to around 20 GPa [57]. To verify whether these effects are a result of changes to the A<sub>1g</sub> mode or the influence of nonhydrostatic pressure conditions, we undertook high-pressure Raman spectroscopy using silicon oil as pressure medium, as shown in figures S2 and S3. The frequency of the A<sub>1g</sub> mode also shows discontinuity at approximately 10 GPa where nonhydrostatic pressure conditions are induced by the silicon oil pressure-transmitting medium. We can thus conclude that the discontinuity in the A<sub>1g</sub> mode is a result of the nonhydrostatic pressure conditions. The intensity of the Raman peak that is located around 380 cm<sup>-1</sup> showed a sharp increase at a pressure of around 22 GPa, as shown in figure S4. This may be a result of the lattice vibrations that could cause the discontinuity in the P–V curve obtained from XRD results at high pressure.

Combined with the high-pressure XRD study, we can conclude that NdAlO<sub>3</sub> maintains its original rhombohedral structure for pressures up to 39.0 GPa.

## 4. Conclusion

In this work, we have investigated the high-pressure structural characteristics of  $\text{RAlO}_3$  ( $\text{R} = \text{Sm}$  or  $\text{Nd}$ ) at room temperature using angle-dispersive synchrotron x-ray powder diffraction. It was found that  $\text{SmAlO}_3$  undergoes an orthorhombic ( $Pnma$ ) to rhombohedral ( $R-3c$ ) phase transition at a pressure of around 10 GPa; this is caused by the reduction in the tilt and distortion of the  $\text{AlO}_6$  octahedra that occurs when they are subject to high pressures. The tilting of the  $\text{AlO}_6$  octahedra in  $\text{NdAlO}_3$  also decreases with increasing pressures. However,  $\text{NdAlO}_3$  maintains its original rhombohedral structure for pressures up to 39.0 GPa. The details of the structural changes that occur in these compounds are useful for determining the electrical and magnetic properties of  $\text{RAlO}_3$  ( $\text{R} = \text{Sm}$  or  $\text{Nd}$ ) at high pressures.

## Acknowledgment

This work was financially supported by the National Natural Science Foundation of China under Grant No. 12204022 and open project of State Key Laboratory of Superhard Materials (Jilin University) (202107).

## Data availability statement

All data that support the findings of this study are included within the article (and any supplementary files).

## References

- [1] Zhao J et al 2021 A combinatory ferroelectric compound bridging simple  $\text{ABO}_3$  and A-site-ordered quadruple perovskite *Nat. Commun.* **12** 1–9
- [2] Terada N, Colin C V, Qureshi N, Hansen T C, Matsubayashi K, Uwatoko Y and Belik A A 2020 Pressure-induced incommensurate antiferromagnetic order in a ferromagnetic B-site ordered double-perovskite  $\text{Lu}_2\text{NiMnO}_6$  *Phys. Rev. B* **102** 094412
- [3] Jin C-Q, Wu X-J, Laffez P, Tatsuki T, Tamura T, Adachi S, Yamauchi N, Koshizuka S and Tanaka S 1995 Superconductivity at 80 K in  $(\text{Sr}, \text{Ca})_3\text{Cu}_2\text{O}_{4+\delta}\text{Cl}_{2-y}$  induced by apical oxygen doping *Nature* **375** 301–3
- [4] Li M et al 2018  $\text{Mn}_2(\text{Fe}_{0.8}\text{Mo}_{0.2})\text{MoO}_6$ : a double perovskite with multiple transition metal sublattice magnetic effects *Chem. Mater.* **30** 4508–14
- [5] Ye X, Wang X, Liu Z, Zhou B, Zhou L, Deng H and Long Y 2022 Emergent physical properties of perovskite-type oxides prepared under high pressure *Dalton Trans.* **51** 1745–53
- [6] Aoyama T, Yamauchi K, Iyama A, Picozzi S, Shimizu K and Kimura T 2014 Giant spin-driven ferroelectric polarization in  $\text{TbMnO}_3$  under high pressure *Nat. Commun.* **5** 4927
- [7] Rozenberg G K, Pasternak M P, Xu W M, Dubrovinsky L S, Carlson S and Taylor R D 2005 Consequences of pressure-instigated spin crossover in  $\text{RFeO}_3$  perovskites; a volume collapse with no symmetry modification *Europhys. Lett.* **71** 228–34
- [8] Gavriliuk A G, Struzhkin V V, Lyubutin I S, Hu M Y and Mao H K 2005 Phase transition with suppression of magnetism in  $\text{BiFeO}_3$  at high pressure *JETP Lett.* **82** 224–7
- [9] Arielly R, Xu W M, Greenberg E, Rozenberg G K, Pasternak M P, Garbarino G, Clark S and Jeanloz R 2011 Intriguing sequence of  $\text{GaFeO}_3$  structures and electronic states to 70 GPa *Phys. Rev. B* **84** 094109
- [10] Haumont R, Bouvier P, Pashkin A, Rabia K, Frank S, Dkhil B, Crichton W A, Kuntscher C A and Kreisel J 2009 Effect of high pressure on multiferroic  $\text{BiFeO}_3$  *Phys. Rev. B* **79** 184110
- [11] Guennou M, Bouvier P, Chen G S, Dkhil B, Haumont R, Garbarino G and Kreisel J 2011 Multiple high-pressure phase transitions in  $\text{BiFeO}_3$  *Phys. Rev. B* **84** 174107
- [12] Bouvier P and Kreisel J 2002 Pressure-induced phase transition in  $\text{LaAlO}_3$  *J. Phys.: Condens. Matter* **14** 3981–91
- [13] Zhao J, Ross N L, Angel R J, Carpenter M A, Howard C J, Pawlak D A and Lukasiewicz T 2009 High-pressure crystallography of rhombohedral  $\text{PrAlO}_3$  perovskite *J. Phys.: Condens. Matter* **21** 235403
- [14] Zeng Z et al 2020 Rare-earth-containing perovskite nanomaterials: design, synthesis, properties and applications *Chem. Soc. Rev.* **49** 1109–43
- [15] Stanek C R, McClellan K J, Levy M R and Grimes R W 2006 Defect behavior in rare earth  $\text{REAlO}_3$  scintillators *J. Appl. Phys.* **99** 113519
- [16] Takahashi T and Iwahara H 1971 Ionic conduction in perovskite-type oxide solid solution and its application to the solid electrolyte fuel cell *Energy Convers.* **11** 105–11
- [17] Liu X, Chen X, Singh D J, Stern A S, Wu J, Petitgirard S, Bina S D and Jacobsen S D 2019 Boron-oxygen complex yields n-type surface layer in semiconducting diamond *Proc. Natl Acad. Sci. USA* **116** 7703–11
- [18] Huang C L and Chen Y C 2002 Low temperature sintering and microwave dielectric properties of  $\text{SmAlO}_3$  ceramics *Mater. Res. Bull.* **37** 563–74
- [19] Tsuji T, Ohashi Y and Yamamura Y 2002 Effect of ionic radius on electrical conductivity of doped  $\text{SmAlO}_3$  perovskite oxide *Solid State Ionics* **154–155** 541–6
- [20] Coutures J and Coutures J P 1984 Etude par rayons X à haute température des transformations polymorphiques des pérovskites *J. Solid State Chem.* **52** 95–100
- [21] Vasylechko L, Senyshyn A and Bismayer U 2009 Chapter 242 perovskite-type aluminates and gallates *Handbook on the Physics and Chemistry of Rare Earths* (Amsterdam: Elsevier) pp 113–295
- [22] Yoshikawa A, Saitow A, Horiuchi H, Shishido T and Fukuda T 1998 Orthorhombic to trigonal phase transition of perovskite-type  $(\text{Nd}, \text{Sm}_{1-x})\text{AlO}_3$  *J. Alloys Compd.* **266** 104–10

- [23] Howard C J, Kennedy B J and Chakoumakos B C 1999 Neutron powder diffraction study of rhombohedral rare-earth aluminates and the rhombohedral to cubic phase transition *J. Phys.: Condens. Matter* **12** 349–65
- [24] Mao H K and Bell P M 1978 Design and varieties of the megabar cell *Year Book* (Washington, DC: Carnegie Institution of Washington) pp 904–8
- [25] Diehl R and Brandt G 1975 Crystal structure refinement of  $\text{YAlO}_3$ , a promising laser material *Mater. Res. Bull.* **10** 85–90
- [26] Marezio M, Dernier P D and Remeika J P 1972 The crystal structures of orthorhombic  $\text{SmAlO}_3$  and of trigonal  $\text{NdAlO}_3$  *J. Solid State Chem.* **4** 11–9
- [27] Cho S-Y, Kim I-T and Hong K S 1999 Microwave dielectric properties and applications of rare-earth aluminates *J. Mater. Res.* **14** 114–9
- [28] Zhao J, Ross N L and Angel R J 2004 Polyhedral control of the rhombohedral to cubic phase transition in  $\text{LaAlO}_3$  perovskite *J. Phys.: Condens. Matter* **16** 8763–73
- [29] Glazer A M 1975 Simple ways of determining perovskite structures *Acta Crystallogr. A* **31** 756–62
- [30] Larson A C and Von Dreele R B 2004 *General Structure Analysis System (GSAS)* (Los Alamos, NM: Los Alamos National Laboratory) pp 86–748
- [31] Chopelas A 1990 Thermal properties of forsterite at mantle pressures derived from vibrational spectroscopy *Phys. Chem. Miner.* **17** 149–56
- [32] Zhao J, Ross N L and Angel R J 2006 Structural evolutions of perovskites under high pressure and high temperature *Physics* **35** 461
- [33] Zhao J, Ross N L and Angel R J 2004 New view of the high-pressure behaviour of  $\text{GdFeO}_3$ -type perovskites *Acta Crystallogr. B* **60** 263–71
- [34] Medarde M et al 1997 Pressure-induced orthorhombic-rhombohedral phase transition in  $\text{NdNiO}_3$  *Physica B: Condensed Matter* **234** 15–17
- [35] Kennedy B J, Vogt T, Martin C D, Parise J B and Hriljac J A 2001 Pressure-induced orthorhombic to rhombohedral phase transition in  $\text{LaGaO}_3$  *J. Phys.: Condens. Matter* **13** L925–30
- [36] Marti W, Fischer P, Altorfer F, Scheel H J and Tadin M 1994 Crystal structures and phase transitions of orthorhombic and rhombohedral  $\text{RGaO}_3$  ( $\text{R} = \text{La, Pr, Nd}$ ) investigated by neutron powder diffraction *J. Phys.: Condens. Matter* **6** 127–35
- [37] Lehnert H, Boysen H, Schneider J, Frey F, Hohlwein D, Radaelli P and Ehrenberg H 2000 A powder diffraction study of the phase transition in  $\text{LaAlO}_3$  *Z. Kristallogr. Cryst. Mater.* **215** 536–41
- [38] García-Muñoz J L, Rodríguez-Carvajal J, Lacorre P and Torrance J B 1992 Neutron-diffraction study of  $\text{RNiO}_3$  ( $\text{R} = \text{La, Pr, Nd, Sm}$ ): electronically induced structural changes across the metal-insulator transition *Phys. Rev. B* **46** 4414
- [39] Angel R J, Zhao J, Ross N L, Jakeways C V, Redfern S A T and Berkowski M 2007 High-pressure structural evolution of a perovskite solid solution  $(\text{La}_{1-x}, \text{Nd}_x)\text{GaO}_3$  *J. Solid State Chem.* **180** 3408–24
- [40] Ross N L, Zhao J and Angel R J 2004 High-pressure structural behavior of  $\text{GdAlO}_3$  and  $\text{GdFeO}_3$  perovskites *J. Solid State Chem.* **177** 3768–75
- [41] Angel R J, Zhao J and Ross N L 2005 General rules for predicting phase transitions in perovskites due to octahedral tilting *Phys. Rev. Lett.* **95** 025503
- [42] Loa I, Adler P, Grzechnik A, Syassen K, Schwarz U, Hanfland M, Rozenberg G K, Gorodetsky P and Pasternak M P 2001 Pressure-induced quenching of the Jahn–Teller distortion and insulator-to-metal transition in  $\text{LaMnO}_3$  *Phys. Rev. Lett.* **87** 125501
- [43] Chen J M et al 2009 Pressure-induced structural distortion of  $\text{TbMnO}_3$ : a combined x-ray diffraction and x-ray absorption spectroscopy study *Phys. Rev. B* **79** 165110
- [44] Lin C, Zhang Y, Liu J, Li X, Li Y, Tang L and Xiong L 2012 Pressure-induced structural change in orthorhombic perovskite  $\text{GdMnO}_3$  *J. Phys.: Condens. Matter* **24** 115402
- [45] Ross N L, Zhao J and Angel R J 2004 High-pressure single-crystal x-ray diffraction study of  $\text{YAlO}_3$  perovskite *J. Solid State Chem.* **177** 1276–84
- [46] Duffy T S, Shen G, Shu J, Mao H-K, Hemley R J and Singh A K 1999 Elasticity, shear strength, and equation of state of molybdenum and gold from x-ray diffraction under nonhydrostatic compression to 24 GPa *J. Appl. Phys.* **86** 6729–36
- [47] Suda J, Kamishima O, Hamaoka K, Matsubara I, Hattori T and Sato T 2003 The first-order Raman spectra and lattice dynamics for  $\text{YAlO}_3$  crystal *J. Phys. Soc. Japan* **72** 1418–22
- [48] Scott J F and Remeika J P 1970 High-temperature Raman study of samarium aluminate *Phys. Rev. B* **1** 4182
- [49] Saine M C and Husson E 1984 Etude vibrationnelle d'aluminates et de gallates de terres rares-IV. Aluminates de samarium et d'euporium *Spectrochim. Acta A* **40** 733–8
- [50] Chopelas A 2011 Single-crystal Raman spectra of  $\text{YAlO}_3$  and  $\text{GdAlO}_3$ : comparison to several orthorhombic  $\text{ABO}_3$  perovskites *Phys. Chem. Minerals* **38** 709–26
- [51] Piermarini G J, Block S and Barnett J D 1973 Hydrostatic limits in liquids and solids to 100 kbar *J. Appl. Phys.* **44** 5377
- [52] Kenichi T and Singh A K 2006 High-pressure equation of state for Nb with a helium-pressure medium: powder x-ray diffraction experiments *Phys. Rev. B* **73** 224119
- [53] Tohei T, Kuwabara A, Yamamoto T, Oba F and Tanaka I 2005 General rule for displacive phase transitions in perovskite compounds revisited by first principles calculations *Phys. Rev. Lett.* **94** 035502
- [54] Harley R T, Hayes W, Perry A M and Smith S R P 1973 The phase transitions of  $\text{PrAlO}_3$  *J. Phys. C: Solid State Phys.* **6** 2382–400
- [55] Sathe V G and Dubey A 2007 Broken symmetry in  $\text{LaAlO}_3$  single crystal probed by resonant Raman spectroscopy *J. Phys.: Condens. Matter* **19** 382201
- [56] Marcondes S P, Rodrigues J E, Andreetta, Hernandez M and Hernandez A C 2014 Resonance Raman spectroscopy of  $\text{NdAlO}_3$  single-crystal fibers grown by the laser-heated pedestal growth technique *Vib. Spectrosc.* **73** 144–9
- [57] Klotz S, Chervin J C, Munsch P and Le Marchand G 2009 *J. Phys. D: Appl. Phys.* **42** 075413